
Article:
Elsheikh, A., Torrero, J., Rojas, S. et al. (2023) In-situ FTIR spectroscopy investigation of carbon-supported PdAuNi electrocatalysts for ethanol oxidation. Journal of Electroanalytical Chemistry, 928. 116985. ISSN: 1572-6657

https://doi.org/10.1016/j.jelechem.2022.116985

In-situ FTIR spectroscopy investigation of carbon-supported PdAuNi electrocatalysts for ethanol oxidation

Ahmed Elsheikh[a,b], Jorge Torrero[c], Sergio Rojas[c], James McGregor[a]

[a] Department of Chemical & Biological Engineering, University of Sheffield, Sheffield S1 3JD, United Kingdom
[b] Mechanical Engineering Department, Faculty of engineering, South Valley University, Qena 83523, Egypt
[c] Grupo de Energía y Química Sostenibles, Instituto de Catálisis y Petroleoquímica, CSIC, C/Marie Curie 2, 28049, Madrid, Spain

Abstract

This work demonstrates novel *in situ* measurements of direct ethanol fuel cells (DEFCs), and shows that the synthesis procedure can exert a substantial influence over their activity, with exceptional activity demonstrated for a trimetallic PdAuNi/C catalyst prepared via $NaBH_4$-2-propanol reduction (SBIPA). Furthermore, *in situ* Fourier transform infrared (FTIR) spectroscopy shows that the final ethanol electrooxidation reaction (EOR) over all catalysts investigated is acetate, thereby yielding valuable insights into the reaction mechanism. DEFCs present a sustainable net-zero technological solution which can supply diverse energy needs without increasing greenhouse gas (GHG) emissions. Ethanol can be produced from biomass precusors, and therefore its direct application in fuel cells can mitigate climate change and ensure environmental sustainability. In this work, PdAuNi/C catalysts are synthesized via three synthetic routes and applied in EOR. The catalysts are charachrterised via X-ray diffraction (XRD), transmission electron microscopy (TEM), energy-dispersive X-ray spectroscopy (EDX), and X-ray photoelectron spectroscopy (XPS). Their electrocatalytic performance is evaluated by cyclic voltammetry (CV), chronoamperometry (CA), and electrochemical impedance spectroscopy (EIS). SBIPA exhibits excellent electrocatalytic results with an oxidation current peak of 9.6 A/mg_{Pd}. This is 4 times greater than that recorded for its monometallic counterpart prepared via the same procedure. It is, also, over twice as great as the other two trimetallic samples prepared by alternative protocols. Although adding Au and Ni to Pd significantly enhances EOR activity, it does not increase the CO_2 yield of EOR.

Keywords: PdAuNi trimetallic, ethanol oxidation reaction, direct ethanol fuel cells, CO_2 yield

Introduction

Direct ethanol fuel cells (DEFCs) are a sustainable and environment-friendly energy conversion technology that can contribute to the growing energy demands of portable, mobile, and stationary applications [1,2]. The benefits of ethanol include its carbon-neutrality (the carbon dioxide produced in DEFCs is reconsumed by the plants which in turn can be used to produce bioethanol); its ease of storage and transportation as it is liquid-phase at ambient conditions; and its high hydrogen density and low toxicity as compared to methanol. It is also less demanding in terms of transportation and safety requirements when compared with hydrogen [1,3–6]. Furthermore, bioethanol can be produced from wastes and residues, thereby avoiding conflict with food crops. The first DEFCs developed operated using an acidic polymer-exchange membrane (PEM) and required Pt-based catalysts, however these exhibited low performance (96 mW/cm^2 at 90ºC). Subsequently, anion-exchange-membranes (AEM) and non-Pt catalysts have demonstrated superior performance (185 mW/cm^2 at 60 ºC) [2]. The alkaline medium could enhance the fuel cell *redox* reaction kinetics [7–9]. Conversely, the alkaline liquid solution causes progressive carbonation of the solution via reaction of CO_2 and H_2O which could be overcome by a solid AEM. To achieve a high catalytic surface area for the reaction to take place, the active catalyst particles need to be dispersed over a high-surface-area, mesoporous, and inert material such as carbon black [10,11].

Bimetallic and trimetallic alloy catalysts based on Pd and/or Pt bring economic and technical benefits towards fuel cell alcohol oxidation [12–16]. The co-catalyst metals are expected to exercise bifunctional, electronic, and geometric effects on Pd structure and catalytic performance [17]. For instance, adding Ni

to Pd/C to prepare binary PdNi catalysts has been reported to significantly improve EOR catalytic performanc. Moreover, unsupported porous PdNi was found to outperform its Pd counterpart due to the electronic and bifunctional effects of Ni [18]. Zhang *et al.* were able to control PdNi particle size using the microemulsion method and found that Ni promotes EOR by recovering Pd active sites [19]. Various C-supported Pd_xAu_y catalysts were prepared and Au was concluded to segregate into the core of PdAu particle while Pd tends to aggregate towards the surface [20,21]. The same group argued that Au incorporation into Pd lattice exercises a tensile strain and shifts the *d*-band center up. Similar findings regarding adding Au into Pd were also reported elsewhere [22]. However, using the electron-beam irradiation, separate Au and Pd phases have been produced, decreasing the probability of alloy formation [23]. Using the successive reduction of Au followed by Pd, Zhou *et al.* [24] have prepared Au@Pd core@shell structure.

EOR can take place either via C1 (complete) or C2 (partial) oxidation pathways. In the C1 pathway, the breaking of the C-C bond of ethanol takes place leading to the formation of CO_2. This route is the preferred one as the total oxidation of ethanol releases 12 electrons. However, upon the scission of the C-C bond, C1 species, namely CO_{ad} and $CH_{x,ad,}$ are formed and remain strongly adsorbed at the catalyst surface, thus poisoning the catalysts [25,26]. A recent *in-situ* IR study of the EOR with Pd catalysts in alkaline electrolyte indicates that the C-C scission takes place at low potentials, whereas at high potentials, partially oxidized C2 products, mostly acetates, are the most detected species [27]. *In-situ* spectroscopic studies for the identification of the species formed during EOR in an alkaline electrolyte with Pt [28,29] or Pd [30,31] have received some attention from researchers recently. Lai *et al.* [28] studied EOR with Pt (and Au) at different pH values combining *in-situ* IR and Raman spectroscopies and concluded that C-C scission on Pt takes place at low potentials, both in acid and alkaline electrolytes leading to $CH_{x,ad}$ and CO_{ad}. Christensen *et al.* [32] concluded that ethanol oxidation with Pt in alkaline medium produces mainly acetate in solution, irrespective of the potential at which the reaction takes place. However, the authors indicated that the EOR pathway depends on ethanol concentration and concluded that under ethanol starvation conditions; acetate species adsorbed at the Pt surface can be oxidized to CO_2 (forming surface carbonates). As with Pt-based catalysts, the electrochemical activity and stability of Pd catalysts can be improved by adding other metals. Therefore, interest has grown in the studying the alkaline EOR with bimetallic catalysts based on Pd [5,27,33]. Shen *et al.* [34] have investigated final products of EOR over Pd and PdNi catalysts and have noted significant electrocatalytic enhancement on PdNi compared to Pd. However, adding Ni to Pd did not improve the C-C cleavage. The authors have also noted improvement in the CO_2 selectivity by increasing the temperature. The CO_2 selectivity increased from 6% at 60° C to 30 % at 100° C.

Trimetallic supported catalysts, unlike bimetallic ones, are not well-explored in the fuel cell electrocatalysis literature. In general, trimetallic systems are difficult to fully understand and control since many factors (e.g., surface chemistry, *d*-band structure, bulk *vs* surface composition, crystallography, others) contribute to the final outcome in a complex manner. Some previous trimetallic catalysts have given a significant performance compared to their monometallic and bimetallic counterparts [33,35,44,36–43]. In this work, C-supported PdAuNi nanoparticles, the preparation and physical charachterisation of which have been previously described [45] and are briefly outlined in the Data-in-Brief, are evaluated for EOR and the final EOR products are identified using *in-situ* FTIR. This represents the first application of *in-situ* FTIR to analyse the EOR final products on trimetallic catalysts.

Materials and Methods

Chemicals, Catalyst Preparation, and Characterization

The chemicals and methods applied to prepare 3 trimetallic PdAuNi/C electrocatalysts and their respective physiochemical charachterisation have been reported previously [45] and are briefly outlined in the supplementary information. The three samples are $PdAuNi/C_{SBEG}$, $PdAuNi/C_{SBIPA}$, $PdAuNi/C_{3\text{-}step}$ in addition to the monometallic Pd/C_{SBIPA}. The subscripts SBEG, SBIPA, and 3-step are abbreviations of

sodium borohydride – ethylene glycol, sodium borohydride – 2-propanol, and 3-step synthesis protocols, respectively. A brief outline of the synthesis methods and physical chachterisation results is contained in the Data-in-Brief document

Electrochemical Evaluation

The catalyst activity towards EOR was investigated by means of CV, CA, and EIS. A 3-electrode halfcell was assembled for that purpose and the electrolyte was magnetically stirred at 50 rpm. To perform the electrocatalytic tests, a Gamry 600R portable station was used. The working electrode is a glassy carbon electrode (GC Ø 3mm) painted with a thin film of the particular catalyst. The reference and counter electrodes are Hg/HgO (NaOH, 1M), and Pt wire, respectively. To prepare the working electrode, 5 mg of the respective catalyst powder was sonicated in 2 mL of ethanol and 25 µL of Nafion 117® (5%) mixture for 30 min. Meanwhile, the GC electrode surface was polished in two steps by alumina powder (1µm and 0.05 µm) to give a mirror-like shining surface. Then, 5 µL of the catalyst slurry were drop-casted on the GC surface and left a few minutes to dry. This was repeated three more times such that the total slurry drop-casted equalled 20 µL. CV was performed by cycling the potential between -0.8 V and +0.5 V vs Hg/HgO at 50 mV/s and the 20th cycle was chosen to stabilise the current for presentation. The CA was performed at -0.4 V vs Hg/HgO for 1 h. The potentiostatic EIS scans were undertaken between 10 kHz and 0.1 Hz and at 10 mV amplitude. Two potentials (-0.4 V and -0.2 V vs Hg/HgO) were applied. EIS experiments were undertaken in static solution, unlike CV and CA, to improve signal-to-noise.

In-situ FTIR

The *in-situ* FTIR scans were collected using a Nicolet 6700 FT-IR spectrometer. Electrochemical experiments were performed in home-made three-electrode polymethylmethacrylate (PMMA) spectro-electrochemical cell equipped with a CaF_2 prism (spectral region 1000–4000 cm^{-1}) in the bottom and connected to an Autolab potentiostat/galvanostat (PGstat 302 N). A reversible hydrogen electrode (RHE) and an Au wire were used as reference and counter electrodes, respectively. An Au disk (Ø 10 mm) was used as a working electrode. The desired amount of catalyst was deposited onto a gold disk electrode by using an ink; typically, 20 µL of ink, prepared by dispersing the respective catalyst powder (4 mg) in acetone (1 mL) and Nafion (20 µL), was placed on a 10 mm diameter gold disk. Prior to ink deposition, the gold electrode was polished, rinsed with water in an ultrasonic bath, and dried under Ar flow. Measurements were done in both 1 M KOH/H_2O and 1 M KOD/D_2O electrolytes. FTIR spectra were acquired between 3100 and 1200 cm^{-1} with a 4-cm^{-1} resolution. To collect the spectra, 0.5M C_2H_5COH was added to the electrolyte (1 M KOH/H_2O and 1 M KOD/D_2O) and purged with Ar for at least 30 min. Then, the working electrode was pressed against the prism and a reference spectrum (R_0) was collected at a constant potential of 50 mV vs RHE. Once the reference spectrum is stable, a process that generally takes more than 30 min, an LSV program is applied between 0.05 and 1.2 V at a scanning rate of 1 mVs^{-1} while recording IR spectra. Each spectrum was taken by accumulating 64 interferograms. The IR spectra during EOR are reported as the R/R_0 ratio, where R and R_0 are the spectra recorded at the selected and reference potentials, respectively. Therefore, the negative bands (*i.e.,* downward) identify species that are either formed at this potential or that their concentration increases with respect to the R_0 spectrum. On the contrary, the positive (*i.e.,* upward) bands are indicative of the disappearance of species (or to a lower concentration of species) that were formed during the recording of the reference spectrum (R_0).

Results

The raw data required to reproduce these findings are available to download from:
[https://figshare.shef.ac.uk/account/articles/19577542]

Electrochemical Evaluation

Fig. 1.A shows the CV scans of Pd/C_{SBIPA}, $PdAuNi/C_{SBIPA}$, $PdAuNi/C_{SBEG}$, and $PdAuNi/C_{3\text{-}step}$ in addition to a commercial Pt/C (40 Wt.%) from Sigma-Aldrich in 1M KOH. ~~The profile thickness of catalyst CV scans seems close to one another suggesting the double layer at the electrolyte-electrode interface has the same thickness and therefore the same charging/discharging speed [46].~~ Investigating the forward scan, a

typical difference between Pt and Pd in terms of hydrogen adsorption/absorption as has been previously reported was observed [38]. The peak around -600 mV on Pt is due to $H_{ads/des}$ on its surface while this is largely suppressed on Pd surface due to its capacity to absorb hydrogen into its bulk structure instead of undertaking surface reaction. The OH adsorption around -400 mV is more pronounced on Pd/C than all other catalysts. At 0.0 V, the catalyst surface Pd starts to be oxidized which increases with increasing the potential up to the forward scan end. Similar behavior was reported elsewhere [47,48].

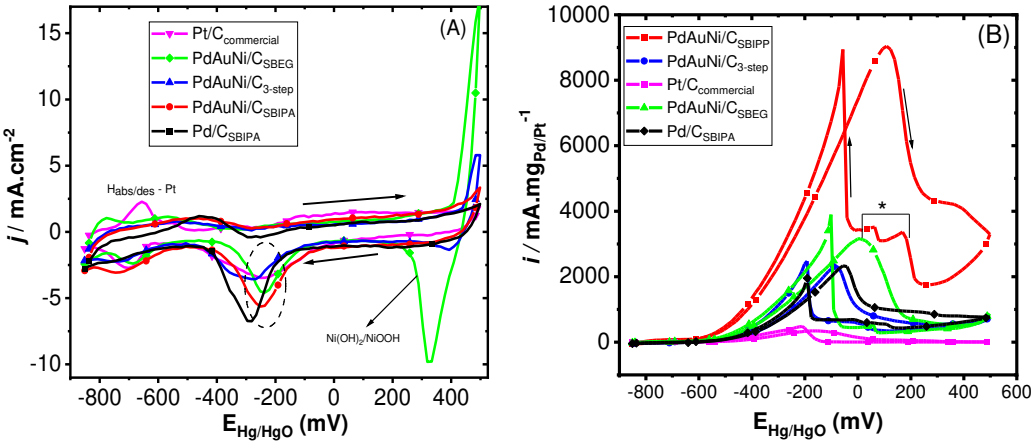

Fig. 1 CV in 1M KOH (A) and 1M KOH+C_2H_5OH (B) of Pd/C_{SBIPA}, Pt/$C_{commercial}$, PdAuNi/C_{SBIPA}, PdAuNi/C_{SBEG}, *and* PdAuNi/$C_{3\text{-}step}$ *at 50 mV/s*

For the trimetallic samples, however, there is a significant current increase towards the end of forward scan; this is due to the oxidation of surface $Ni(OH)_2$ to NiOOH [14,35]. This Ni-associated current increase is highest on PdAuNi/C_{SBEG} followed by PdAuNi/$C_{3\text{-step}}$, and finally PdAuNi/C_{SBIPA}. This is the same order of Ni content in SBEG>3-step>SBIPA according to [45]. Starting the reverse scan, the NiOOH is reduced back to $Ni(OH)_2$ around +300 mV. The surface PdO is reduced at a further lower potential around -280 mV which is shifted approximately 50 mV to higher potential in the case of the trimetallic samples due to Au presence as was reported in [49]. The PdO reduction peak in the reverse scan could be utilized to quantify the electrochemical active surface area (ECSA, cm^2/mg) of the respective four catalysts according to:

$$ECSA = \frac{Q}{0.43 \times [Pd]}$$

Where, Q is the charge extracted by PdO reduction in mC, 0.43 is the charge of reducing one layer of PdO in mC, and [Pd] is the quantity of Pd on the glassy carbon electrode in mg. For the current four catalysts, the ECSA was found 79, 150, 45, and 46 cm^2/mg_{Pd} for Pd/C_{SBIPA}, PdAuNi/C_{SBIPA}, PdAuNi/C_{SBEG}, and PdAuNi/C_{3step}, respectively. Having the highest ECSA implies that PdAuNi/C_{SBIPA} possesses a significant reactive surface sites compared to the other trimetallic and monometallic samples. Moreover, the small ECSA of both PdAuNi/C_{SBEG} and PdAuNi/C_{3step} signies a little Pd surface coverage on those catalysts to less than one third of PdAuNi/C_{SBIPA} and approximately half of Pd/C_{SBIPA}. Surprisingly, the addition of Au and Ni using the SBEG and 3step prtotcols has decreased the Pd ECSA. This suggests PdAuNi/C_{SBIPA} is probably the most active catalyst due to the presence of more Pd active sites on its surface.

Fig. 1.B shows the CV scans in 1 M KOH+C_2H_5OH at 50 mV/s. The 1M concentration was chosen because it gives a critical balance between the OH and ethoxy species concentrations on the catalyst surface according to [47]. Moreover, this curve is normalized by the Pd weight in the electrode since it is the active EOR component. Another CV curve is added in the supplementary information document (Fig. 3) that is normalized by the electrode area. Starting the forward scan, the $H_{ads/abs}$ is substantially

suppressed – on all catalysts – by ethoxy adsorption [7,14]. On Pd/C, the adsorbed ethoxy oxidation starts at -490 mV with the OH adsorption start. As the adsorbed OH quantity increases, with the applied potential, the oxidation current and removal of ethoxy from Pd surface sites grow until no further OH is adsorbed at approximately 0.0 V [7]. Above that, the oxidation current decreases due to active surface depletion due to Pd surface oxidation. A sharp current increase, coinciding with the PdO reduction potential in Fig. 1 for each corresponding catalyst, in the reverse scan is noted due to the recovery of Pd active sites and consequent adsorption of organic species from the solution, which is, also, reported in [50,51]. This backward current peak at -200 mV is smaller than the forward current peak at 0 V for Pd/C_{SBIPA} which suggests a tolerance towards poisoning species. For PdAuNi/C_{SBIPA}, the addition of Au and Ni into Pd has added a remarkable benefit towards the oxidation of ethanol on Pd verified by the current increase compared to Pd/C_{SBIPA}. While the oxidation current peak of the latter is 1800 mA/mg_{Pd}, it is 9600 mA/mg_{Pd} of the former. Moreover, PdAuNi/C_{SBIPA} achieves current density significantly higher than many published catalysts of diverse natures [18,20,46–48,52,53]. This could be explained by the smaller particle size [45]. Furthermore, the oxidation onset potential on PdAuNi/C_{SBIPA} is approximately 100 mV lower than that of Pd/C_{SBIPA} which implies the EOR overvoltage of PdAuNi/C_{SBIPA} is 100 mV lower than that of Pd/C_{SBIPA}. This could be attributed to the Pd electronic configuration after alloying with Au and Ni [45]. According to XRD analysis, the addition of Au and Ni to Pd has exercised a lattice strain on Pd lattice making it more active towards EOR. Furthermore, XPS studies have verified the improved Pd air stability. Adding Ni and Au increases the Pd electron energy as it gains electrons from Ni and/or Au , as indicated by shifting the Pd 3d binding energy to a lower value. This has likely resulted in decreasing the adsorption bond strength between Pd and ethanol species. Additionally, the PdAuNi/C_{SBIPA} surface contains more Pd than Ni or Au, thereby ensuring a high surface concentration and hence presenting aubundant active sites for EOR. Similar arguments could be made, to some extent, for the SBEG trimetallic sample; however its Ni-rich surface has adversely impacted its EOR performance as compared to PdAuNi/C_{SBIPA}. That is why a significant EOR current decrease is noted and a higher backward current peak than the forward is also obtained with PdAuNi/C_{SBEG}. Additionally, its agglomeration potential – indicated by TEM and XRD [45] – is higher than the SBIPA trimetallic sample. All of these observations signal increased blocking of the few Pd active sites on PdAuNi/C_{SBEG} as EOR proceeds. As for PdAuNi/$C_{3\text{-step}}$, the catalytic performance towards EOR is inferior to that of the other two intermetallic samples even though its surface contains more Pd than Ni and Au [45]. However, its step-wise reduction during synthesis has resulted in the largest particle size according to TEM and XRD analyses [45]. Furthermore, its XRD pattern [45] implies the production of an Au-like structure and Au is not EOR-active. Pt/$C_{commercial}$ gives the lowest catalytic performance towards EOR.

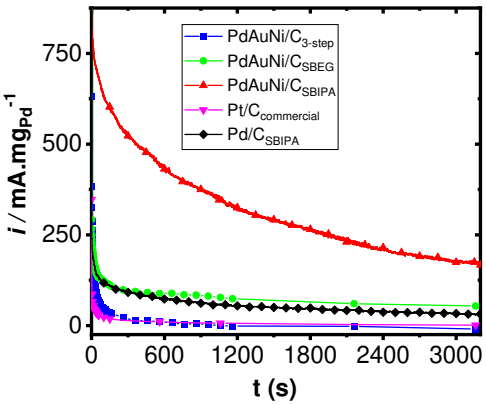

Fig. 2 (A) CA scans at -400 mV vs Hg/HgO in 1M KOH+C_2H_5OH of Pd/C_{SBIPA}, Pt/$C_{commercial}$, PdAuNi/C_{SBIPA}, PdAuNi/C_{SBEG}, and PdAuNi/$C_{3\text{-step}}$

Fig. 2 shows the chronoamperometry (CA) scans recorded for 1h at -400 mV vs Hg/HgO. This potential was chosen because it is close to the start of EOR with the OH adsorption on all catalysts. The current

obtained with PdAuNi/C_{SBIPA} is significantly higher than the other catalysts due to its physiochemical properties including Pd-surface abundance, smaller particle size, and alloying with Au and Ni, which all could promote EOR [35,45,48]. Its current density however declines faster than the other samples, implying rapid degradation of Pd active sites due to EOR poisoning species. Pd/C_{SBIPA}, on the other hand, generates much less current than its trimetallic counterpart, but it shows a higher current stability that experiences a negligible decline over the 1-h scan period. Similar behavior is noted with PdAuNi/C_{SBEG}. The 3-step trimetallic and commercial Pt samples show very weak activity, stability and tolerance towards EOR implying a very fast blocking and degradation of the catalytic sites.

FTIR measurements

The products formed during the EOR, and their evolution with potential have been monitored using EC-FITR in H_2O and D_2O electrolytes. This was done to avoid the interference of the strong vibrational bands of H_2O around ca. 3500 cm^{-1} and 1600 cm^{-1} [32]. These spectral regions contain information about certain species formed during the EOR, especially acetyls and other C2 species. In order to prevent the overlapping of those bands, we have conducted the EOR experiments in deuterated electrolytes, since D_2O (or OD) bands do not appear in the said spectral regions [54]. On the other hand, the use of deuterated electrolytes can hinder the identification of CO_{ad} and CO_2, which can be observed in the spectra recorded in protonated electrolyte. Therefore, we recorded the EOR experiments in both solvents with each catalyst.

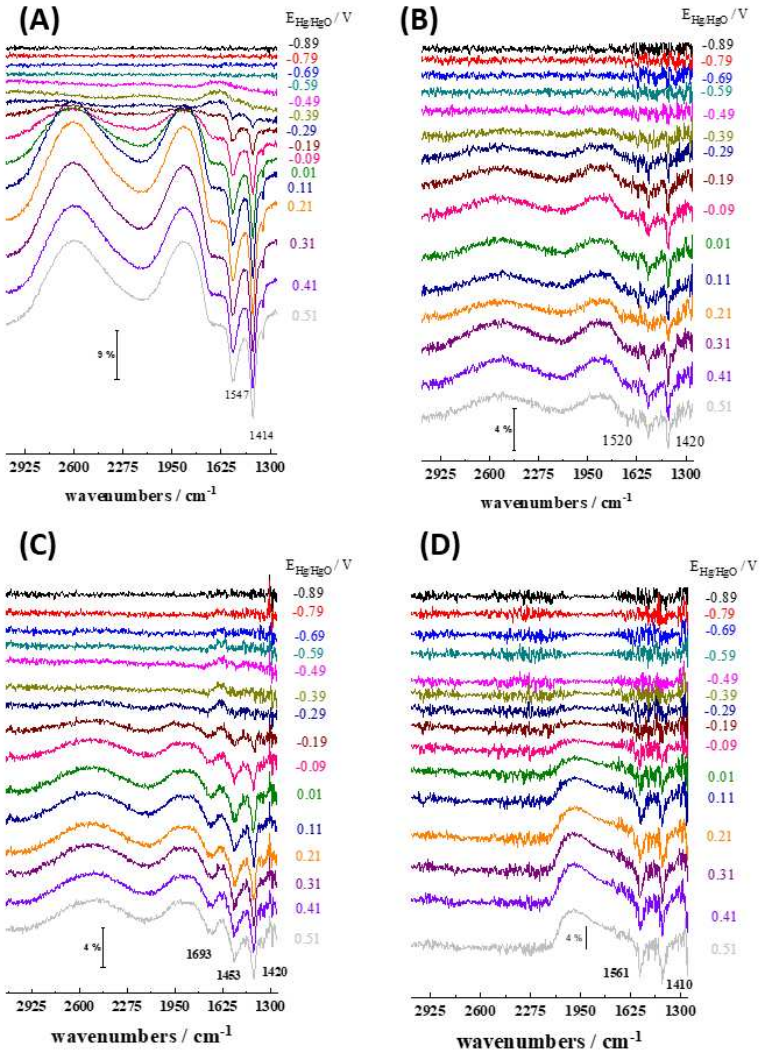

Fig. 3 FTIR spectra for EOR 0.5 M EtOH in 0.5 M KOH/H_2O recorded between -0.89 V and 0.51 V at 1 mVs^{-1} for A)Pd/C_{SBIPA}, B)PdAuNi/C_{3steps}, C)PdAuNi/C_{SBEG} and D)PdAuNi/C_{SBIPA}

First, Fig. 3 shows the spectra for the EOR recorded in aqueous electrolyte (H_2O/KOH) for the catalysts under study. The main bands observed in the spectra are centered at ca. 1690 and 1410 cm^{-1} (in most cases) and are visible at high potentials (E > -290 mV). These bands are usually ascribed to acetates [55]. The spectra fail to show the presence of CO_{ad} species or CO_2 (this latter finding is not surprising since CO_2 is not stable in alkaline electrolyte). The spectra recorded for all samples display similar bands, however, certain differences can be observed. Although the spectra for Pd/C_{SBIPA} in Fig. 3 fail to show bands for CO_{ad} and CO_2 species, we observed such *very weak* bands in some of the EOR studies. For instance, the spectra depicted in Fig. 4 show a weak feature at ca. 2080 cm^{-1} corresponding to the formation of linear-bounded CO_{ad} on Pd [27,56,57] and a small negative band at 2343 cm^{-1} ascribed to the presence of CO_2 [54]. The observation of CO_2 indicates that the electrolyte is becoming acidified during the EOR due to OH^- consumption [58]. These bands were never observed in the spectra of the other three polymetallic catalysts. This observation indicates that the EOR with the monometallic Pd catalyst goes (in part) through the C1 pathway [51], which is breaking the C-C bond of ethanol.

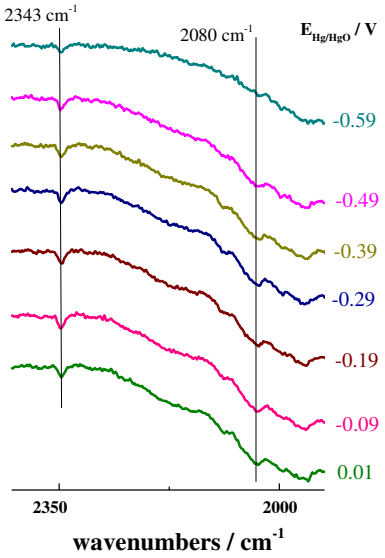

Fig. 4 Magnification for FTIR spectra for EOR 0.5 M EtOH in 0.5 M KOH/H_2O recorded between -0.89 V and 0.51 V at 1 mVs^{-1} for Pd/C_{SBIPA}

The spectra recorded during the EOR in deuterated electrolyte are shown in *Fig. 5*. A magnification of the spectral region of interest is shown in *Fig. 6*. The bands within the 1700-1300 cm^{-1} region are better resolved than in H_2O electrolyte. Also, a set of positive going bands around 3000 cm^{-1} are observed. These bands indicate the consumption of CH_x species is most likely due to the oxidation of ethanol. The trimetallic samples display two main bands, at ca. 1554 and 1414 cm^{-1}. These bands indicate the presence of acetates, which are the main products of EOR with the trimetallic catalysts. These bands are also observed in the spectra of the monometallic catalyst. In addition, the spectra for the monometallic catalyst shows two further bands, one at 1622 cm^{-1} and a further band at 1360 cm^{-1}. The latter band, which appears only at high potentials E > 0.01 V, is ascribed to the formation of carbonates, indicating the total oxidation of ethanol to CO_2 (or CO_3^{2-} in alkaline electrolyte) [31,32]. The bands at ca. 1622 cm^{-1} are usually ascribed to the formation of acetyl species, which have been usually seen as intermediate species during the scission of the C-C bond of ethanol.

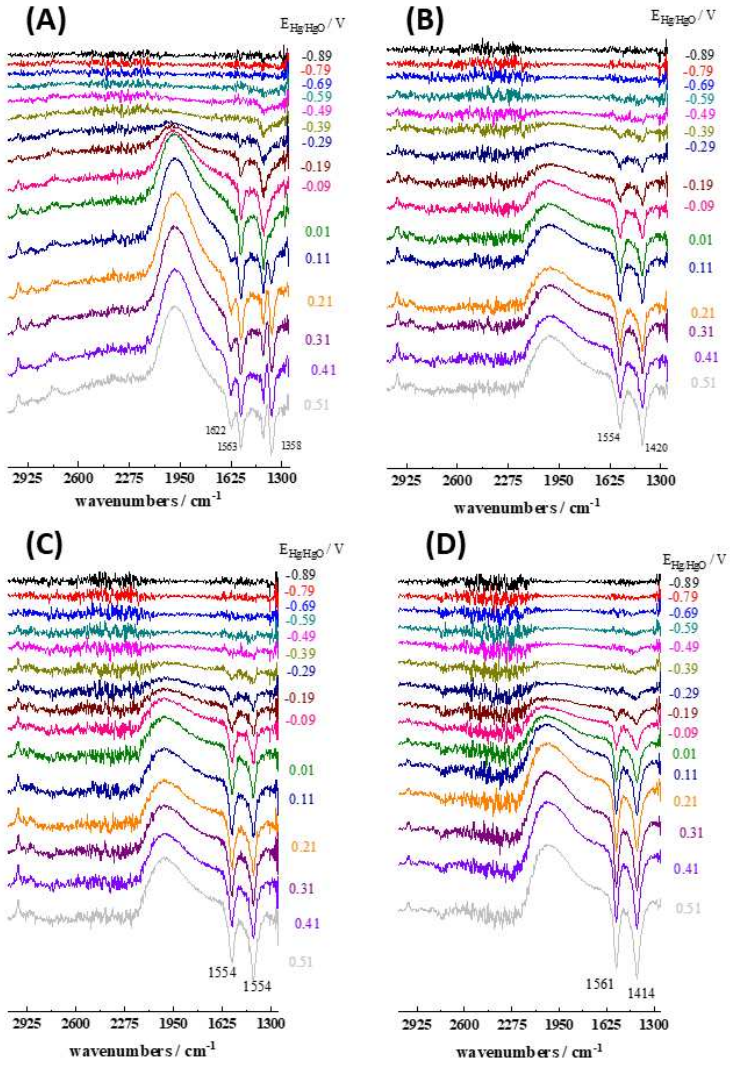

Fig. 5 FTIR spectra for EOR 0.5 M EtOH in 0.5 M KOD/D_2O recorded between 0.05 V and 1.2 V at 1 mVs^{-1} for A) Pd/C_{SBIPA}, B) PdAuNi/$C_{3\text{-steps}}$, C) PdAuNi/C_{SBEG} and D) PdAuNi/C_{SBIPA}.

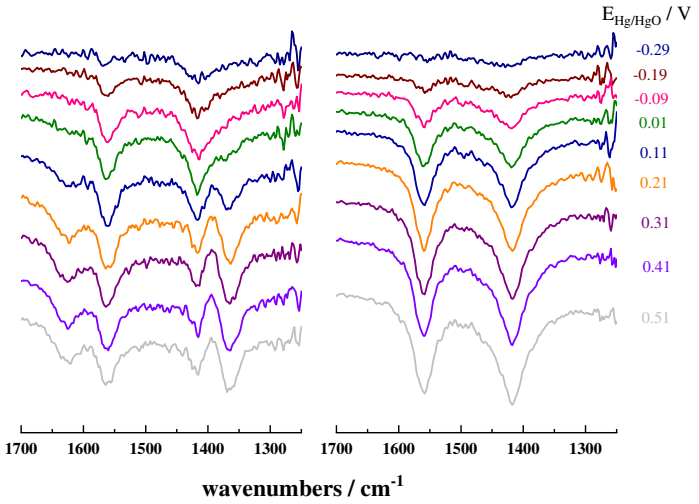

Fig. 6 Magnification of the IR region of the spectra of Pd/C_{SBIPA} and PdAuNi/C_{SBIPA} between 1700 and 1250 cm^{-1} for E ≥ -0.29 V in Fig. 5

The IR spectra, in Fig. 7, show that acetates are the main species formed during the EOR in alkaline electrolyte. The potential at which acetates are observed in the IR spectra coincide with the onset potential for the EOR observed in the cyclic voltammograms recorded ex-situ, namely -490, -490, -540 and -590 mV for Pd/C_{SBIPA}, PdAuNi/C_{3step}, PdAuNi/C_{SBEG} and PdAuNi/C_{SBIPA}, respectively.

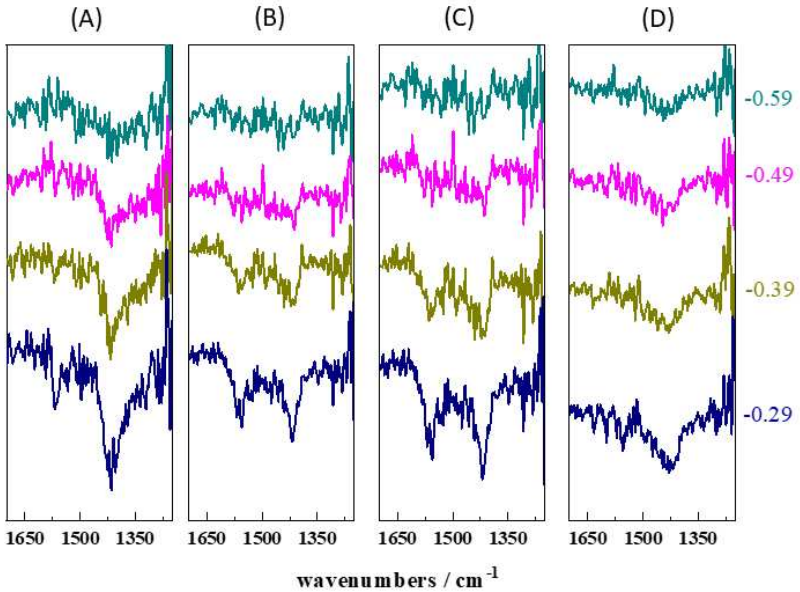

Fig. 7 Magnification of the IR region of the spectra in Fig. 3 between -0.59 V and -0.29 V for 1200 – 1700 cm^{-1} region of (A) Pd/C_{SBIPA}, (B) PdAuNi/C_{3step}, (C) PdAuNi/C_{SBEG}, and (D) PdAuNi/C_{SBIPA}

The FTIR measurements, therefore, confirm the weak potential of Pd-based electrocatalysts to break the ethanol C-C bond. The underlying reasons could include the missing oxygen species adsorption at lower potential values at which the C-C bond cleavage could happen. Furthermore, the OH adsoption occurs at high potential where the C2 pathway is preferered to the C1 one. Eventually, the only final product detected is acetate. Furthermore, the enhanced catalytic performance of PdAuNi/C_{SBIPA} could be attributed

only to promoting the C2 pathway activity and yielding higher quantities of acetate from the fed ethanol compared to the the monometallic Pd/C_{SBIPA} and other trimetallic samples.

The selectivity towards the production of C2 (acetates) or C1 (carbonates) for each catalyst was assessed by monitoring the evolution of the intensity of the bands at 1415 cm^{-1} (acetate) and 1390 cm^{-1} (carbonates) with the applied potential, respectively. As shown in *Fig 8 (left panel)*, all catalysts under study produce acetates, with PdAuNi/C_{SBIPA} showing the highest production of acetates, especially at high potentials. On the other hand, the production of carbonates has been only observed with Pd/C_{SBIPA} at E > 0.01V (Fig. 8 right panel). These results indicate that the trimetallic catalysts show higher selectivity for the C2 reaction pathway than monometallic Pd/C_{SBIPA}, showing both acetates (especially at low potentials) and carbonates (at high potential).

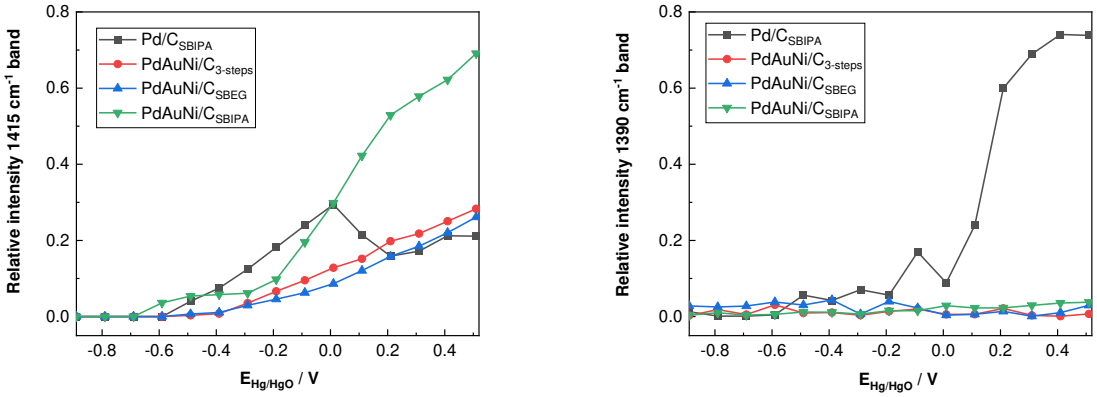

Fig. 8 Evolution of the intensity of the IR bands at 1415 cm^{-1} (left panel, acetates) and 1390 cm^{-1} (right panel, acrbonates) with the increasing potential during the EOR for the catalysts studied in this work

The FTIR measurements, therefore, confirm the weak potential of Pd-based electrocatalysts to break the ethanol C-C bond. The underlying reasons could include the missing oxygen species adsorption at lower potential values at which the C-C bond cleavage could happen, and that OH adsorption occurs at high potential where the C2 pathway is preferred to the C1 one. Eventually, the only final product detected is acetate. Furthermore, the enhanced catalytic performance of PdAuNi/C_{SBIPA} could be attributed to promoting the C2 pathway activity and yielding higher quantities of acetate from the fed ethanol compared to the monometallic Pd/C_{SBIPA} and other trimetallic samples. In light of the FTIR results, the EOR C2 pathway seems to prevail over the C1 one as acetate is the only final product on all catalysts. Therefore the following EOR reaction could be suggested for current catalysts:

$$CH_3CH_2OH + 4OH^- \rightarrow CH_3COOH + 3H_2O + 4e^-$$

Conclusions

The ethanol oxidation performance of three previously-reported PdAuNi/C catalysts and *in-situ* analysis of the final oxidation products were performed. The SBIPA trimetallic sample has shown a remarkable catalytic performance (9.6 A/mg_{Pd} oxidation current peak) toward EOR at least 2.3 times higher than the other catalysts (the SBEG and 3-step trimetallic- and Pd/C_{SBIPA} samples). Adding Ni and Au has significantly promoted Pd EOR kinetics. . The FTIR spectroscopy results show acetate as the main EOR product in all catalysts. The EOR with the trimetallic catalysts produce acetates, without evidence of forming C1 species. Acetates are also the main products of the EOR on the monometallic catalyst

Pd/C_{SBIPA}. However, traces of C1 species (namely CO_{ad} and carbonates) are formed during the EOR with the monometallic catalyst. Thus, the Pd EOR activity could be significantly enhanced by adding Ni and Au, while its CO_2 selectivity remains unchanged or is reduced.

Acknowledgements

Ahmed Elsheikh is grateful to Newton-Mosharafa Fund (Grant No NM J08/15) for the financial support of his Ph.D. studies. Proyecto ENE2016-77055-C3-3-R financiado por MCIN/AEI /10.13039/501100011033 y por FEDER Una manera de hacer Europa

References

[1] L. An, T.S. Zhao, Transport phenomena in alkaline direct ethanol fuel cells for sustainable energy production, J. Power Sources. 341 (2017). https://doi.org/10.1016/j.jpowsour.2016.11.117.

[2] L. An, T.S.S. Zhao, Y.S.S. Li, Carbon-neutral sustainable energy technology: Direct ethanol fuel cells, Renew. Sustain. Energy Rev. 50 (2015) 1462–1468. https://doi.org/10.1016/j.rser.2015.05.074.

[3] G.L. Soloveichik, G.L. Soloveichik Review, Liquid fuel cells, Beilstein J. Nanotechnol. 5 (2014) 1399–1418. https://doi.org/10.3762/bjnano.5.153.

[4] B.C. Ong, S.K. Kamarudin, S. Basri, Direct liquid fuel cells: A review, Int. J. Hydrogen Energy. 42 (2017) 10142–10157. https://doi.org/10.1016/j.ijhydene.2017.01.117.

[5] A. Brouzgou, A. Podias, P. Tsiakaras, PEMFCs and AEMFCs directly fed with ethanol: A current status comparative review, J. Appl. Electrochem. 43 (2013) 119–136. https://doi.org/10.1007/s10800-012-0513-2.

[6] S.P.S.P.S.S. Badwal, S. Giddey, A. Kulkarni, J. Goel, S. Basu, Direct ethanol fuel cells for transport and stationary applications – A comprehensive review, Appl. Energy. 145 (2015) 80–103. https://doi.org/10.1016/J.APENERGY.2015.02.002.

[7] Y. Wang, S. Zou, W.-B. Cai, Recent Advances on Electro-Oxidation of Ethanol on Pt- and Pd-Based Catalysts: From Reaction Mechanisms to Catalytic Materials, Catalysts. 5 (2015) 1507–1534. https://doi.org/10.3390/catal5031507.

[8] G. Merle, M. Wessling, K. Nijmeijer, Anion exchange membranes for alkaline fuel cells: A review, J. Memb. Sci. 377 (2011) 1–35. https://doi.org/10.1016/j.memsci.2011.04.043.

[9] J. Qi, N. Benipal, C. Liang, W. Li, PdAg/CNT catalyzed alcohol oxidation reaction for high-performance anion exchange membrane direct alcohol fuel cell (alcohol = methanol, ethanol, ethylene glycol and glycerol), Appl. Catal. B Environ. 199 (2016) 494–503. https://doi.org/10.1016/j.apcatb.2016.06.055.

[10] L.P.R. Moraes, B.R. Matos, C. Radtke, E.I. Santiago, F.C. Fonseca, S.C. Amico, C.F. Malfatti, Synthesis and performance of palladium-based electrocatalysts in alkaline direct ethanol fuel cell, Int. J. Hydrogen Energy. 41 (2016) 6457–6468. https://doi.org/10.1016/j.ijhydene.2016.02.150.

[11] E. Antolini, Carbon supports for low-temperature fuel cell catalysts, Appl. Catal. B Environ. 88 (2009) 1–24. https://doi.org/10.1016/J.APCATB.2008.09.030.

[12] A.B. Delpeuch, F. Maillard, M. Chatenet, P. Soudant, C. Cremers, A. Bach Delpeuch, F. Maillard, M. Chatenet, P. Soudant, C. Cremers, Ethanol oxidation reaction (EOR) investigation on Pt/C, Rh/C, and Pt-based bi- and tri-metallic electrocatalysts: A DEMS and in situ FTIR study, Appl. Catal. B Environ. 181 (2016) 672–680. https://doi.org/10.1016/J.APCATB.2015.08.041.

[13] M. Li, A. Kowal, K. Sasaki, N. Marinkovic, D. Su, E. Korach, P. Liu, R.R. Adzic, Ethanol oxidation on the ternary Pt-Rh-SnO2/C electrocatalysts with varied Pt:Rh:Sn ratios, Electrochim. Acta. 55 (2010) 4331–4338. https://doi.org/10.1016/j.electacta.2009.12.071.

[14] M.D. Obradović, Z.M. Stančić, U.Č. Lačnjevac, V.V.V.R. Radmilović, A. Gavrilović-Wohlmuther, V.V.V.R. Radmilović, S.L. Gojković, Electrochemical oxidation of ethanol on palladium-nickel nanocatalyst in alkaline media, Appl. Catal. B Environ. 189 (2016) 110–118. https://doi.org/10.1016/J.APCATB.2016.02.039.

[15] R.S. Amin, R.M.A. Hameed, K.M. El-Khatib, M.E. Youssef, R.M. Abdel Hameed, K.M. El-Khatib, M. Elsayed Youssef, R.M.A. Hameed, K.M. El-Khatib, M.E. Youssef, Electrocatalytic activity of nanostructured Ni and Pd-Ni on Vulcan XC-72R carbon black for methanol oxidation in alkaline medium, Int. J. Hydrogen Energy. 39 (2014) 2026–2041. https://doi.org/10.1016/j.ijhydene.2013.11.033.
[16] H. Xu, P. Song, C. Fernandez, J. Wang, M. Zhu, Y. Shiraishi, Y. Du, Sophisticated Construction of Binary PdPb Alloy Nanocubes as Robust Electrocatalysts toward Ethylene Glycol and Glycerol Oxidation, ACS Appl. Mater. Interfaces. 10 (2018) 12659–12665. https://doi.org/10.1021/acsami.8b00532.
[17] H. Xu, H. Shang, C. Wang, Y. Du, Low-Dimensional Metallic Nanomaterials for Advanced Electrocatalysis, Adv. Funct. Mater. 30 (2020) 1–33. https://doi.org/10.1002/adfm.202006317.
[18] Y. Feng, D. Bin, B. Yan, Y. Du, T. Majima, W. Zhou, Porous bimetallic PdNi catalyst with high electrocatalytic activity for ethanol electrooxidation, J. Colloid Interface Sci. 493 (2017) 190–197. https://doi.org/10.1016/j.jcis.2017.01.035.
[19] Z. Zhang, L. Xin, K. Sun, W. Li, Pd–Ni electrocatalysts for efficient ethanol oxidation reaction in alkaline electrolyte, Int. J. Hydrogen Energy. 36 (2011) 12686–12697. https://doi.org/10.1016/j.ijhydene.2011.06.141.
[20] Y.-Y. Feng, Z.-H. Liu, Y. Xu, P. Wang, W.-H. Wang, D.-S. Kong, Highly active PdAu alloy catalysts for ethanol electro-oxidation, J. Power Sources. 232 (2013) 99–105. https://doi.org/10.1016/j.jpowsour.2013.01.013.
[21] Z. Yin, M. Chi, Q. Zhu, D. Ma, J. Sun, X. Bao, Supported bimetallic PdAu nanoparticles with superior electrocatalytic activity towards methanol oxidation, J. Mater. Chem. A. 1 (2013) 9157. https://doi.org/10.1039/c3ta11592e.
[22] S. Zhang, M. Qing, H. Zhang, Y. Tian, Electrocatalytic oxidation of formic acid on functional MWCNTs supported nanostructured Pd–Au catalyst, Electrochem. Commun. 11 (2009) 2249–2252. https://doi.org/10.1016/J.ELECOM.2009.10.001.
[23] A.N. Geraldes, D.F. da Silva, E.S. Pino, J.C.M. da Silva, R.F.B. de Souza, P. Hammer, E.V. Spinacé, A.O. Neto, M. Linardi, M.C. dos Santos, Ethanol electro-oxidation in an alkaline medium using Pd/C, Au/C and PdAu/C electrocatalysts prepared by electron beam irradiation, Electrochim. Acta. 111 (2013) 455–465. https://doi.org/10.1016/j.electacta.2013.08.021.
[24] W. Zhou, J.Y. Lee, Highly active core–shell Au@Pd catalyst for formic acid electrooxidation, Electrochem. Commun. 9 (2007) 1725–1729. https://doi.org/10.1016/J.ELECOM.2007.03.016.
[25] Y. Zhang, G. Chang, S. Liu, J. Tian, L. Wang, W. Lu, X. Qin, X. Sun, Microwave-assisted, environmentally friendly, one-pot preparation of Pd nanoparticles/graphene nanocomposites and their application in electrocatalytic oxidation of methanol, Catal. Sci. Technol. 1 (2011) 1636–1640. https://doi.org/10.1039/C1CY00296A.
[26] H. Xu, B. Yan, K. Zhang, C. Wang, J. Zhong, S. Li, Y. Du, P. Yang, PVP-stabilized PdAu nanowire networks prepared in different solvents endowed with high electrocatalytic activities for the oxidation of ethylene glycol and isopropanol, Colloids Surfaces A Physicochem. Eng. Asp. 522 (2017) 335–345. https://doi.org/https://doi.org/10.1016/j.colsurfa.2017.03.015.
[27] M. Farsadrooh, J. Torrero, L. Pascual, M.A.M.A. Peña, M. Retuerto, S. Rojas, Two-dimensional Pd-nanosheets as efficient electrocatalysts for ethanol electrooxidation. Evidences of the C–C scission at low potentials, Appl. Catal. B Environ. 237 (2018) 866–875. https://doi.org/10.1016/j.apcatb.2018.06.051.
[28] S.C.S.S. Lai, S.E.F.F. Kleijn, F.T.Z.Z. Öztürk, V.C. van Rees Vellinga, J. Koning, P. Rodriguez, M.T.M.M. Koper, V.C. Van, R. Vellinga, J. Koning, P. Rodriguez, M.T.M.M. Koper, Effects of electrolyte pH and composition on the ethanol electro-oxidation reaction, Catal. Today. 154 (2010) 92–104. https://doi.org/10.1016/j.cattod.2010.01.060.
[29] M. López-Atalaya, E. Morallón, F. Cases, J.L. Vázquez, J.M. Pérez, Electrochemical oxidation of ethanol on Pt(hkl) basal surfaces in NaOH and Na2CO3 media, J. Power Sources. 52 (1994) 109–117. https://doi.org/https://doi.org/10.1016/0378-7753(94)01950-9.

[30] U. Martinez, A. Serov, M. Padilla, P. Atanassov, Mechanistic Insight into Oxide-Promoted Palladium Catalysts for the Electro-Oxidation of Ethanol, ChemSusChem. 7 (2014) 2351–2357. https://doi.org/https://doi.org/10.1002/cssc.201402062.
[31] X. Fang, L. Wang, P.K. Shen, G. Cui, C. Bianchini, An in situ Fourier transform infrared spectroelectrochemical study on ethanol electrooxidation on Pd in alkaline solution, J. Power Sources. 195 (2010) 1375–1378. https://doi.org/10.1016/j.jpowsour.2009.09.025.
[32] P.A. Christensen, S.W.M. Jones, A. Hamnett, In Situ FTIR Studies of Ethanol Oxidation at Polycrystalline Pt in Alkaline Solution, J. Phys. Chem. C. 116 (2012) 24681–24689. https://doi.org/10.1021/jp308783y.
[33] W. Zhu, J. Ke, S.-B. Wang, J. Ren, H.-H. Wang, Z.-Y. Zhou, R. Si, Y.-W. Zhang, C.-H. Yan, Shaping Single-Crystalline Trimetallic Pt–Pd–Rh Nanocrystals toward High-Efficiency C–C Splitting of Ethanol in Conversion to CO2, ACS Catal. 5 (2015) 1995–2008. https://doi.org/10.1021/cs5018419.
[34] S.Y.Y. Shen, T.S.S. Zhao, Q.X.X. Wu, Product analysis of the ethanol oxidation reaction on palladium-based catalysts in an anion-exchange membrane fuel cell environment, Int. J. Hydrogen Energy. 37 (2012) 575–582. https://doi.org/http://dx.doi.org/10.1016/j.ijhydene.2011.09.077.
[35] A. Dutta, J. Datta, Outstanding Catalyst Performance of PdAuNi Nanoparticles for the Anodic Reaction in an Alkaline Direct Ethanol (with Anion-Exchange Membrane) Fuel Cell, J. Phys. Chem. C. 116 (2012) 25677–25688. https://doi.org/10.1021/jp305323s.
[36] S. Beyhan, J.-M. Léger, F. Kadırgan, Pronounced synergetic effect of the nano-sized PtSnNi/C catalyst for ethanol oxidation in direct ethanol fuel cell, Appl. Catal. B Environ. 130–131 (2013) 305–313. https://doi.org/10.1016/j.apcatb.2012.11.007.
[37] B. Ulas, A. Caglar, O. Sahin, H. Kivrak, Composition dependent activity of PdAgNi alloy catalysts for formic acid electrooxidation, J. Colloid Interface Sci. 532 (2018) 47–57. https://doi.org/10.1016/j.jcis.2018.07.120.
[38] L.S. Parreira, J.C.M. da Silva, M. D'Villa -Silva, F.C. Simões, S. Garcia, I. Gaubeur, M.A.L. Cordeiro, E.R. Leite, M.C. dos Santos, L. Silveira Parreira, J. César Martins da Silva, V. -Silva, F. Carmona Simões, S. Garcia, I. Gaubeur, M. Aurélio Liutheviciene Cordeiro, E. Roberto Leite, M. Coelho dos Santos, PtSnNi/C nanoparticle electrocatalysts for the ethanol oxidation reaction: Ni stability study, Electrochim. Acta. 96 (2013) 243–252. https://doi.org/10.1016/j.electacta.2013.02.054.
[39] M. Yurderi, A. Bulut, M. Zahmakiran, M. Kaya, Carbon supported trimetallic PdNiAg nanoparticles as highly active, selective and reusable catalyst in the formic acid decomposition, Appl. Catal. B Environ. 160–161 (2014) 514–524. https://doi.org/10.1016/j.apcatb.2014.06.004.
[40] G. Sharma, D. Kumar, A. Kumar, H. Al-Muhtaseb, D. Pathania, M. Naushad, G. Tessema Mola, Revolution from monometallic to trimetallic nanoparticle composites, various synthesis methods and their applications: A review, (2017). https://doi.org/10.1016/j.msec.2016.11.002.
[41] C. Shang, W. Hong, J. Wang, E. Wang, Carbon supported trimetallic nickel-palladium-gold hollow nanoparticles with superior catalytic activity for methanol electrooxidation electrooxidation, J. Power Sources. 285 (2015) 12–15. https://www-sciencedirect-com.sheffield.idm.oclc.org/science/article/pii/S037877531500508X (accessed May 11, 2019).
[42] H. Xu, J. Wang, B. Yan, S. Li, C. Wang, Y. Shiraishi, P. Yang, Y. Du, Facile construction of fascinating trimetallic PdAuAg nanocages with exceptional ethylene glycol and glycerol oxidation activity, Nanoscale. 9 (2017) 17004–17012. https://doi.org/10.1039/c7nr06737b.
[43] S. Hu, F. Munoz, J. Noborikawa, J. Haan, L. Scudiero, S. Ha, Carbon supported Pd-based bimetallic and trimetallic catalyst for formic acid electrochemical oxidation, Appl. Catal. B Environ. 180 (2016) 758–765. https://doi.org/10.1016/j.apcatb.2015.07.023.
[44] W. Lu, X. Xia, X. Wei, M. Li, M. Zeng, J. Guo, S. Cheng, Nanoengineering 2D Dendritic PdAgPt Nanoalloys with Edge-Enriched Active Sites for Enhanced Alcohol Electroxidation and Electrocatalytic Hydrogen Evolution, ACS Appl. Mater. Interfaces. 12 (2020) 21569–21578. https://doi.org/10.1021/acsami.0c01690.

[45] A.M.A. Elsheikh, G. Backović, R.C.P. Oliveira, C.A.C. Sequeira, J. McGregor, B. Šljukić, D.M.F. Santos, Carbon-supported trimetallic catalysts (Pdauni/c) for borohydride oxidation reaction, Nanomaterials. 11 (2021). https://doi.org/10.3390/nano11061441.
[46] F. Zhu, M. Wang, Y. He, G. Ma, Z. Zhang, X. Wang, A comparative study of elemental additives (Ni, Co and Ag) on electrocatalytic activity improvement of PdSn-based catalysts for ethanol and formic acid electro-oxidation, Electrochim. Acta. 148 (2014) 291–301. https://doi.org/10.1016/j.electacta.2014.10.062.
[47] L. Ma, D. Chu, R. Chen, Comparison of ethanol electro-oxidation on Pt/C and Pd/C catalysts in alkaline media, Int. J. Hydrogen Energy. 37 (2012) 11185–11194. https://doi.org/10.1016/j.ijhydene.2012.04.132.
[48] P.P.-C. Su, H.-S.H. Chen, T.T.-Y. Chen, C.-W.C. Liu, C.-H. Lee, J.-F. Lee, T.-S. Chan, K.-W. Wang, Enhancement of electrochemical properties of Pd/C catalysts toward ethanol oxidation reaction in alkaline solution through Ni and Au alloying, Int. J. Hydrogen Energy. 38 (2013) 4474–4482. https://doi.org/10.1016/J.IJHYDENE.2013.01.173.
[49] D.J. Chadderdon, L. Xin, J. Qi, Y. Qiu, P. Krishna, K.L. More, W. Li, Electrocatalytic oxidation of 5-hydroxymethylfurfural to 2,5-furandicarboxylic acid on supported Au and Pd bimetallic nanoparticles, Green Chem. 16 (2014) 3778–3786. https://doi.org/10.1039/c4gc00401a.
[50] N. Erini, P. Krause, M. Gliech, R. Yang, Y. Huang, P. Strasser, Comparative assessment of synthetic strategies toward active platinumerhodiumetin electrocatalysts for efficient ethanol electro-oxidation, J. Power Sources. 294 (2015) 299–304. https://doi.org/10.1016/j.jpowsour.2015.06.042.
[51] J. Torrero, M. Montiel, M.A.M.A. Peña, P. Ocón, S. Rojas, Insights on the electrooxidation of ethanol with Pd-based catalysts in alkaline electrolyte, Int. J. Hydrogen Energy. 4 (2019) 1–8. https://doi.org/10.1016/j.ijhydene.2019.10.124.
[52] C. Zhu, D. Wen, M. Oschatz, M. Holzschuh, W. Liu, A.-K.K. Herrmann, F. Simon, S. Kaskel, A. Eychmüller, Kinetically controlled synthesis of PdNi bimetallic porous nanostructures with enhanced electrocatalytic activity, Small. 11 (2015) 1430–1434. https://doi.org/10.1002/smll.201401432.
[53] H. Lv, L. Sun, L. Zou, D. Xu, H. Yao, B. Liu, Electrode for proton exchange membrane fuel cells: A review, Chem. Sci. 10 (2019) 1986–1993. https://doi.org/10.1039/C8SC04696D.
[54] J. Torrero, F.J. Pérez-Alonso, M.A. Peña, C. Domínguez, A.O. Al-Youbi, S.A. Al-Thabaiti, S.N. Basahel, A.A. Alshehri, S. Rojas, In Situ Infrared Study of the Electrooxidation of Ethanol and Acetaldehyde in Acid Electrolyte, ChemElectroChem. 3 (2016). https://doi.org/10.1002/celc.201600136.
[55] S. Beyhan, K. Uosaki, J.M. Feliu, E. Herrero, Electrochemical and in situ FTIR studies of ethanol adsorption and oxidation on gold single crystal electrodes in alkaline media, J. Electroanal. Chem. 707 (2013) 89–94. https://doi.org/10.1016/j.jelechem.2013.08.034.
[56] Y.-Y. Yang, J. Ren, Q.-X. Li, Z.-Y. Zhou, S.-G. Sun, W.-B. Cai, Electrocatalysis of Ethanol on a Pd Electrode in Alkaline Media: An in Situ Attenuated Total Reflection Surface-Enhanced Infrared Absorption Spectroscopy Study, ACS Catal. 4 (2014) 798–803. https://doi.org/10.1021/cs401198t.
[57] S.D. Ebbesen, B.L. Mojet, L. Lefferts, The influence of water and pH on adsorption and oxidation of CO on Pd/Al2 O3 —an investigation by attenuated total reflection infrared spectroscopy, Phys. Chem. Chem. Phys. 11 (2009) 641–649. https://doi.org/10.1039/B814605E.
[58] M.C. Figueiredo, R.M. Arán-Ais, V. Climent, T. Kallio, J.M. Feliu, Evidence of Local pH Changes during Ethanol Oxidation at Pt Electrodes in Alkaline Media, ChemElectroChem. 2 (2015) 1254–1258. https://doi.org/https://doi.org/10.1002/celc.201500151.